



Hydrothermally synthesized nickel cobalt oxide for bifunctional electrochemical supercapacitor and nonenzymatic glucose biosensor

O. C. Pore^{1,2} · A. V. Fulari³ · V. J. Fulari² · G. M. Lohar¹

Received: 8 October 2022 / Accepted: 5 December 2022 / Published online: 15 December 2022
© The Author(s), under exclusive licence to Springer-Verlag GmbH, DE part of Springer Nature 2022

Abstract

Herein, various nickel cobalt oxide nanostructures with different Ni concentrations are prepared via a hydrothermal route followed by annealing process for an electrochemical supercapacitor as well as a nonenzymatic glucose biosensor. The electrode synthesized on carbon cloth using $\text{Ni}_{0.9}\text{Co}_{2.1}\text{O}_4$ nanosheet-like morphology showed a maximum 516.51 F g^{-1} specific capacitance at 10 mV s^{-1} scan rate and the cyclic stability of 87.7% over 2000 GCD cycles. The electrode prepared with $\text{Ni}_{0.3}\text{Co}_{2.7}\text{O}_4$ on CC offered a linear response from 0 to 0.3 mM glucose concentration and exhibited a maximum of $759.5 \mu\text{A mM}^{-1} \text{ cm}^{-2}$ glucose sensitivity.

Keywords Hydrothermal · Nickel cobalt oxide · Supercapacitor · Nonenzymatic glucose sensing

1 Introduction

Nowadays, human beings have suffered from problems such as deficiency of fossil fuels, global warming, and pollution. Hence, it is essential to produce energy from renewable sources like solar, tide, and wind. Also, low-cost, environmentally friendly, advanced energy storage and conversion devices must store energy harvested from renewable resources [1–4]. There are different energy storage devices such as conventional capacitors, biofuel, lithium-ion batteries (LIBs), and supercapacitors [5–10]. Supercapacitors, also called electrochemical supercapacitors, are the most desirable candidates for energy storage. Their unique electrochemical properties like high power density, excellent coulombic efficiency, and high cyclic stability make them compatible with other energy storage devices. Still, supercapacitors suffered from low energy density as compared to LIBs. So, to improve the energy density of supercapacitors,

efforts have been made to develop novel electrodes with suitable synthesis strategies [9, 11–14].

The different conducting polymers [15], transition metal oxides, and transition metal hydroxides such as Co_3O_4 [12], NiO [16], $\text{Co}(\text{OH})_2$ [17], $\text{Ni}(\text{OH})_2$ [18, 19], RuO_2 [20], MnO_2 [9, 21] have been widely studied as an electrode for pseudocapacitors. The transition metal oxides deliver higher specific capacitance as compared to conducting polymers due to multi-electron redox reactions. In addition, ternary metal oxides, because of their better electrical conductivity and rich redox-active sites, shows better supercapacitor performance than single metal oxide [22]. Spinel nickel cobalt oxide (NiCo_2O_4) has been widely used as high-performance capacitive electrode material in recent years. It shows better electrical conductivity, relatively lower electron transport activation energy, and better electrochemical activity than cobalt oxide (Co_3O_4) and nickel oxide (NiO) [22, 23]. This high electrical conductivity and improved specific capacitance of NiCo_2O_4 are because of contributions from both the Co and Ni ions with diverse valence states.

Researchers have made many efforts to enhance electrochemical performance by developing nickel cobalt oxide with different morphologies. Waghmode et al. [24] synthesized NiCo_2O_4 nanoflowers by chemical bath deposition method and observed capacitance was 610 F g^{-1} at 1 mA cm^{-2} . Ma et al. [25], with the solution precursor thermal spray method, developed NiCo_2O_4 hollow microspheres, which showed specific capacitance 902 F g^{-1} at

✉ G. M. Lohar
gauravlohar24@gmail.com

¹ Department of Physics, Lal Bahadur Shastri College of Arts, Science and Commerce, Satara, MH 415002, India

² Department of Physics, Holography and Materials Research Laboratory, Shivaji University, Kolhapur, MH 416004, India

³ Division of Physics and Semiconductor Science, Dongguk University, Seoul 04620, South Korea

1 A g⁻¹. Qi et al. [26] synthesized NiCo₂O₄ hollow microspheres by a hydrothermal method which showed a specific capacitance of 720 F g⁻¹ at 2 A g⁻¹. Saravanakumar et al. [27] synthesized NiCo₂O₄ nanoparticles via hydrothermal route and observed specific capacitance was 294 F g⁻¹ at 1 A g⁻¹. Uke et al. [28] synthesized NiCo₂O₄ nanomorphs by hydrothermal method and observed specific capacitance was 479 F g⁻¹ with better retention.

In the medical industries, quality control in food and clinical diagnosis of diabetes; rapid, accurate, and sensitive detection of glucose is essential [29, 30]. Recently, sensitive and selective enzyme-based sensors have been studied for glucose sensing. But they cannot be reused for continuous glucose detection. They suffer from low stability, which limits their use in actual applications [31, 32]. The other method, i.e., nonenzymatic glucose biosensing, exhibited high stability, sensitivity, and reproducibility. Qin et al. [33] developed NiCo₂O₄ nanowires with the help of hydrothermal and calcination treatment. The prepared glucose sensor shows 72.4 μM mM⁻¹ cm⁻² glucose sensitivity and 0.37 μM detection limit. Hussain et al. [34] prepared NiCo₂O₄ nanoneedles on nickel foam and it exhibited a sensitivity of 91.34 mV/decade with a response time of less than 10 s. Yang et al. [35] synthesized hollow nanorods of NiCo₂O₄ with the help of a sacrificial template accelerate hydrolysis method achieved 1685.1 μM mM⁻¹ cm⁻² glucose sensitivity. Ma et al. [36] developed NiCo₂O₄ nanowrinkles on graphene oxide sheets with a hydrothermal route. NiCo₂O₄ nanowrinkles achieved a glucose sensitivity of 548.9 μM mM⁻¹ cm⁻².

In the present investigation, the different nickel cobalt oxide nanostructures by varying concentrations of Ni in cobalt oxide are prepared by the hydrothermal route and studied for both supercapacitor and glucose biosensing applications. The electrodes are synthesized using a flexible carbon cloth (CC) current collector with a simple doctor blade method. The synthesized Ni_{0.9}Co_{2.1}O₄ nanosheets exhibited 516.51 F g⁻¹ specific capacitance at 10 mV s⁻¹ with a capacity retention of 87.7% over 2000 cycles. At the same time, Ni_{0.3}Co_{2.7}O₄ nanosheets showed a maximum 759.5 μA mM⁻¹ cm⁻² glucose sensitivity with a linear response from 0.0 to 0.3 mM glucose concentration.

2 Experimental

2.1 Preparation of different Nickel cobalt oxide powders

The nickel cobalt oxide powders with different Ni percentages were synthesized by the hydrothermal route and then calcination. In a synthesis of Co₃O₄, 0.1 M

Co(NO₃)₂·6H₂O and 0.2 M of urea were added in Double distilled water (DDW). NH₃ was added to the solution dropwise up to pH = 11 and stirred for 30 min. Afterward, the whole solution was poured into a Teflon liner (100 mL), fitted in a stainless-steel autoclave, and the reaction was carried out at 180 °C for 18 h. Then, the autoclave was cooled to room temperature, and reaction products were cleaned with DDW and ethanol many times and dried at 60 °C in the oven for 12 h. Lastly, the prepared powder was annealed at 400 °C for 2 h. Similarly, powders with different Ni concentrations were synthesized by adding different percentages of Ni as 0%, 10%, 20%, 30%, and 40% in Co₃O₄. Based on the various percentages of Ni precursor, the stoichiometries are observed in Co₃O₄, Ni_{0.3}Co_{2.7}O₄, Ni_{0.6}Co_{2.4}O₄, Ni_{0.9}Co_{2.1}O₄, and Ni_{1.2}Co_{1.8}O₄, respectively.

2.2 Preparation of electrode

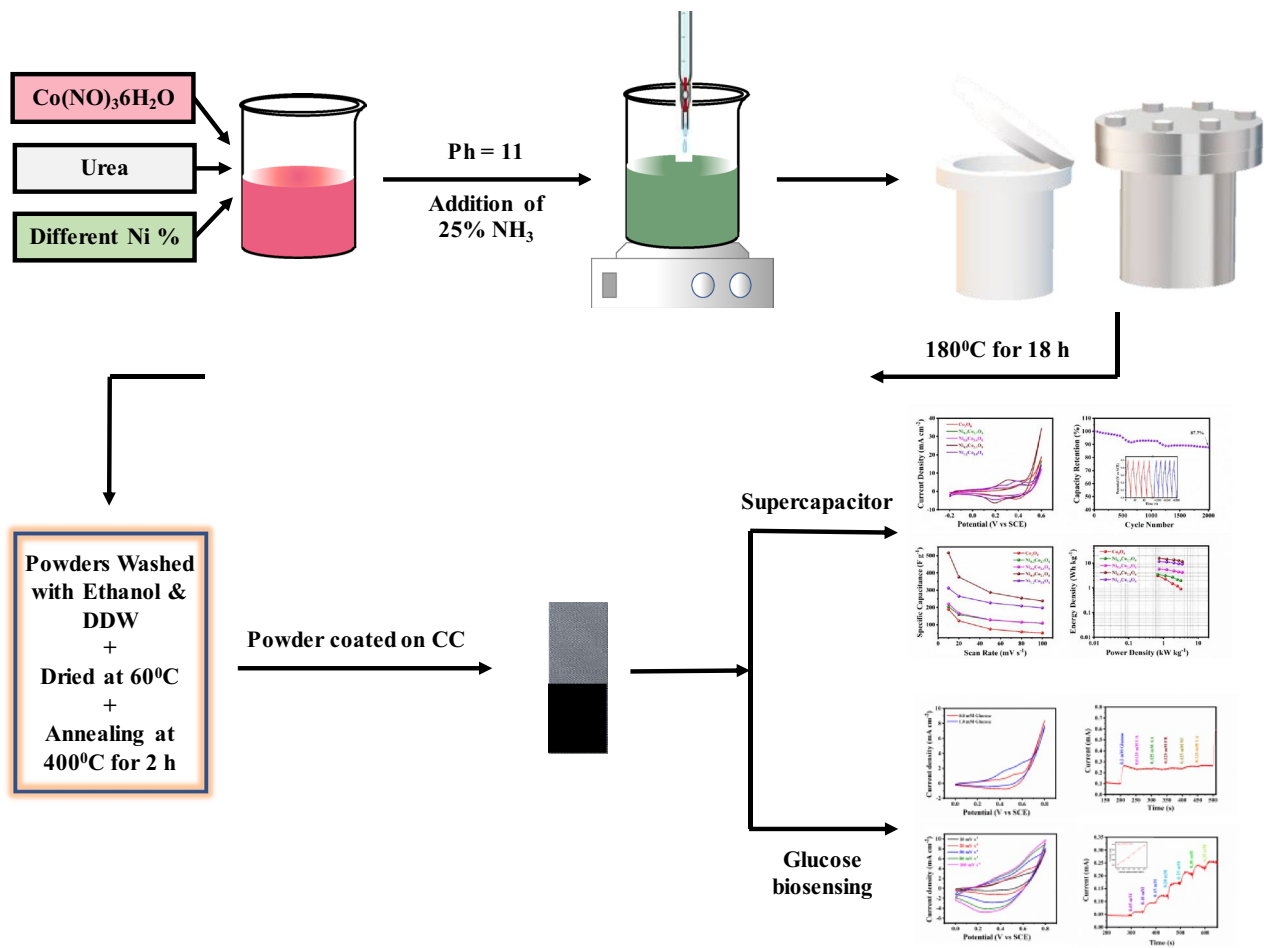
In an ultrasonication bath, a piece of CC (2 cm × 1 cm) was cleaned with ethanol, acetone, and DDW each for 10 min respectively, and dried overnight at 60 °C in the oven. The actual electrode was prepared by mixing prepared powders (active material), PVDF as a binder, and a carbon black ratio of 80:10:10. Then, a sufficient amount of NMP solvent was mixed to obtain a uniform slurry. Then, the prepared slurry was coated on CC (1 cm × 1 cm) and subjected to 80 °C in a hot air oven for 12 h. These prepared electrodes were used for electrochemical supercapacitor and nonenzymatic glucose biosensor study. The experimental procedure can be presented in Scheme 1.

XRD pattern of prepared powders recorded using a Bruker D2 phaser tabletop model under Cu Kα radiation. FTIR was taken by Lambda-7600, Australia. The morphology was analyzed using FE-SEM from the Mira-3, Tescan, Brno-Czech Republic. Biologic SP-300 electrochemical workstation used for electrochemical supercapacitor and glucose biosensor study.

3 Results and discussion

3.1 XRD study

Figure 1A presents the XRD patterns of different nickel cobalt oxide nanostructures. The observed d-spacing values in XRD patterns are associated with standard JCPDS card 01-080-1543 for Co₃O₄ and 01-073-1702 after adding different Ni concentrations. The peaks are observed at an angle, 64.98, 59.19, 44.68, 36.79, 31.16, 18.94° which are applied to the cubic structure and assigned to the (440),



Scheme 1 Schematic representation of overall experimental procedure

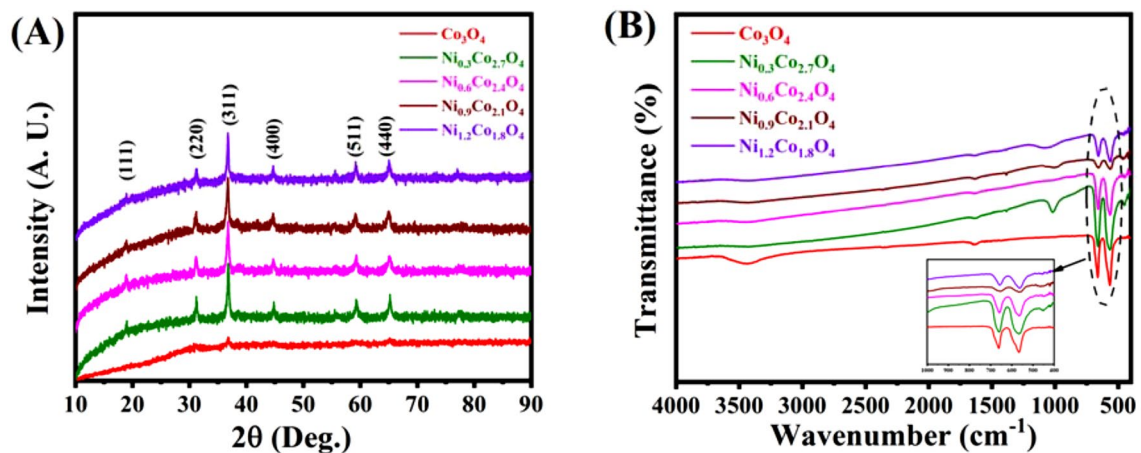


Fig. 1 Structural analysis of nickel cobalt oxide **A** XRD patterns and **B** FTIR of nickel cobalt oxide powders with different Ni concentrations

(511), (400), (311), (220), and (111) crystal planes, respectively. The crystallite size is calculated using the Scherer's formula [7, 37]. The calculated values for average crystallite

size are 34.18, 36.61, 43.10, 30.96, and 34.18 nm for Co_3O_4 , $\text{Ni}_{0.3}\text{Co}_{2.7}\text{O}_4$, $\text{Ni}_{0.6}\text{Co}_{2.4}\text{O}_4$, $\text{Ni}_{0.9}\text{Co}_{2.1}\text{O}_4$, and $\text{Ni}_{1.2}\text{Co}_{1.8}\text{O}_4$, respectively.

3.2 FTIR study

The different nickel cobalt oxide powders were further characterized by the FTIR study. Figure 1B presents the FTIR spectra of all synthesized nickel cobalt oxide powders. The FTIR spectra display two sharp peaks at about 661 cm^{-1} and 565 cm^{-1} which originated from Co–O bonds (stretching vibrations), confirming the formation of Co_3O_4 [38, 39]. As the percentage of Ni increases, these two peaks shift towards a higher wavenumber. The corresponding change in the peak is mentioned in supplementary information Table S1. The relatively weak peaks at about 1632 and 3432 cm^{-1} are associated with the O–H bending and stretching mode of vibration of water [14, 40, 41].

3.3 FE-SEM study

Figure 2 shows FE-SEM pictures and EDS analysis of different nickel cobalt oxide powders. The Co_3O_4 in Fig. 2A

shows nanosheets like nature. As the different percentages of Ni are added into Co_3O_4 , surface modifications are observed. In Fig. 2B, the nanosheet-like morphologies are observed, which are merged. As the percentage of Ni increases, the nanosheets are incorporated a lot in Fig. 2C. The flakes are started covered with nanoparticles in Fig. 2D, and finally, the number of nanoparticles increased as shown in Fig. 2E corresponding to the $\text{Ni}_{1.2}\text{Co}_{1.8}\text{O}_4$. Figure 2F shows the EDS spectra of $\text{Ni}_{1.2}\text{Co}_{1.8}\text{O}_4$, which confirms the presence of Ni, Co, and O. Figure 2G–I presents the elemental distribution of Ni, Co, and O, respectively.

3.4 EIS study

The electrochemical behavior at the electrode–electrolyte interface was studied by using the EIS study. Figure 3 presents the EIS study of synthesized Co_3O_4 , $\text{Ni}_{0.3}\text{Co}_{2.7}\text{O}_4$, $\text{Ni}_{0.6}\text{Co}_{2.4}\text{O}_4$, $\text{Ni}_{0.9}\text{Co}_{2.1}\text{O}_4$, and $\text{Ni}_{1.2}\text{Co}_{1.8}\text{O}_4$ electrodes. EIS spectra were recorded within the 1 MHz to 0.1 Hz frequency

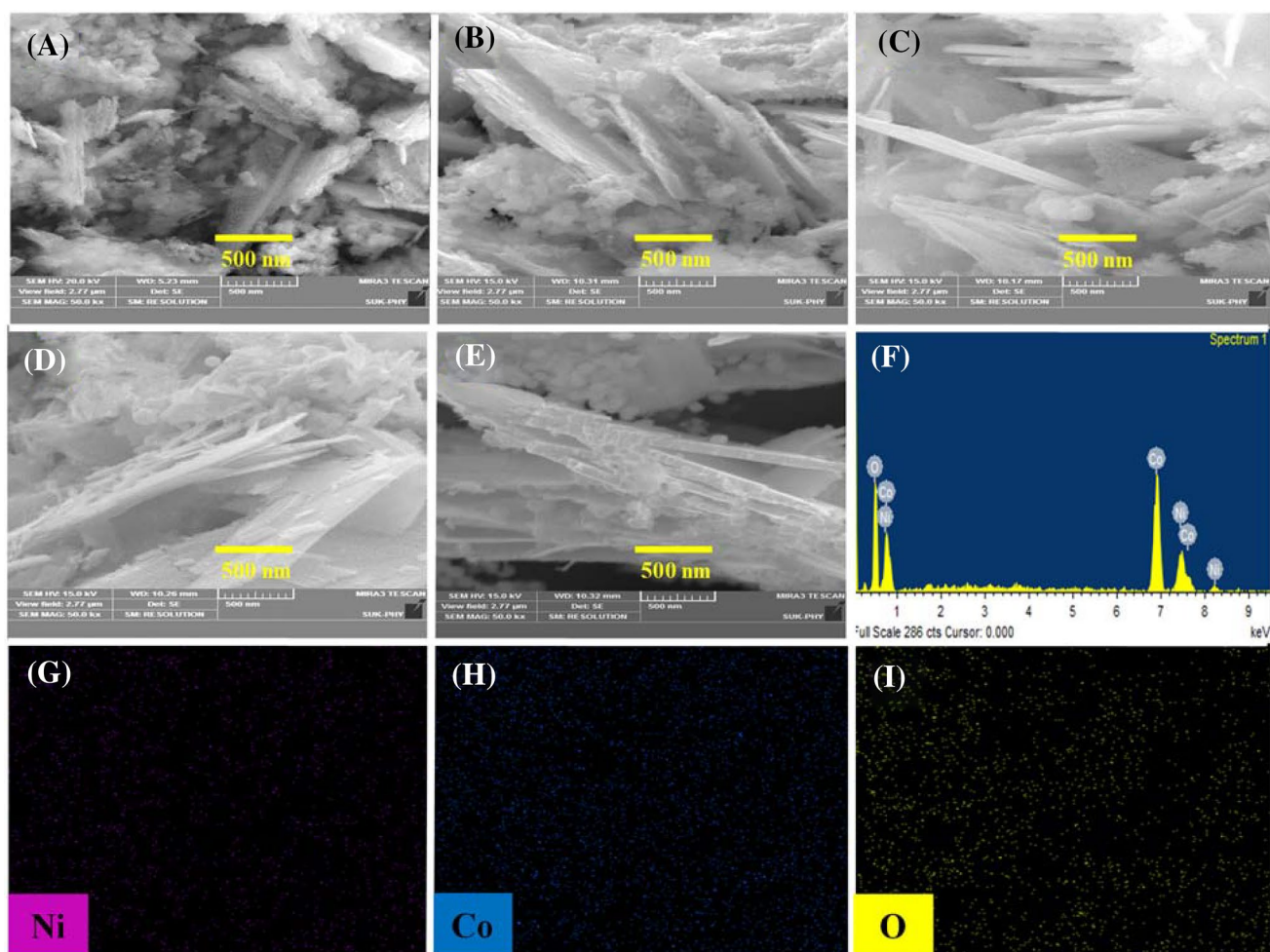


Fig. 2 Morphology of nickel cobalt oxide powders. **A–E** FE-SEM images of Co_3O_4 , $\text{Ni}_{0.3}\text{Co}_{2.7}\text{O}_4$, $\text{Ni}_{0.6}\text{Co}_{2.4}\text{O}_4$, $\text{Ni}_{0.9}\text{Co}_{2.1}\text{O}_4$, and $\text{Ni}_{1.2}\text{Co}_{1.8}\text{O}_4$ powders, respectively. **F** EDS image of $\text{Ni}_{0.9}\text{Co}_{2.1}\text{O}_4$ powder. **G–I** Element distribution images of Ni, Co, and O, respectively

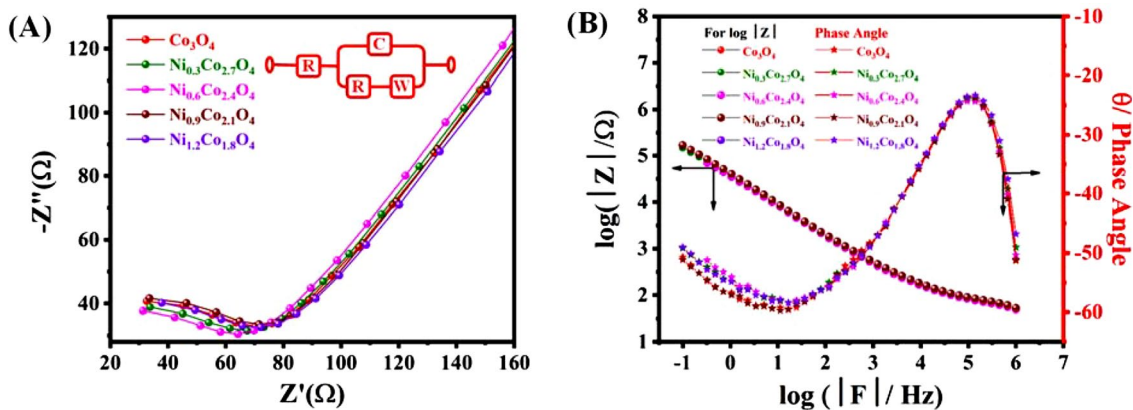


Fig. 3 EIS analysis of all nickel cobalt oxide powders. **A** Nyquist plot (Inset: Equivalent circuit diagram). **B** Bode plot of different nickel cobalt oxide powders with different Ni concentrations

range in 1 M KOH electrolyte at an applied potential of 20 mV. Figure 3A presents the Nyquist plots of Co_3O_4 , $\text{Ni}_{0.3}\text{Co}_{2.7}\text{O}_4$, $\text{Ni}_{0.6}\text{Co}_{2.4}\text{O}_4$, $\text{Ni}_{0.9}\text{Co}_{2.1}\text{O}_4$, and $\text{Ni}_{1.2}\text{Co}_{1.8}\text{O}_4$ electrodes. The inset of Fig. 3A shows the corresponding fitted circuit diagram. The charge transfer resistance values for Co_3O_4 , $\text{Ni}_{0.3}\text{Co}_{2.7}\text{O}_4$, $\text{Ni}_{0.6}\text{Co}_{2.4}\text{O}_4$, $\text{Ni}_{0.9}\text{Co}_{2.1}\text{O}_4$, and $\text{Ni}_{1.2}\text{Co}_{1.8}\text{O}_4$ electrodes are 61.20, 60.86, 58.21, 55.87, and 62.03 $\Omega \text{ cm}^{-2}$, respectively. The lower R_{ct} values reveal better electrical conductivity and good adhesion of coated

material with the current collector [42]. Figure 3B presents the Bode plot of Co_3O_4 , $\text{Ni}_{0.3}\text{Co}_{2.7}\text{O}_4$, $\text{Ni}_{0.6}\text{Co}_{2.4}\text{O}_4$, $\text{Ni}_{0.9}\text{Co}_{2.1}\text{O}_4$, and $\text{Ni}_{1.2}\text{Co}_{1.8}\text{O}_4$ electrodes, respectively.

3.5 Electrochemical supercapacitor study

The three-electrode system with SCE as a reference electrode, platinum wire counter electrode, and prepared CC electrodes as a working electrode is used to study

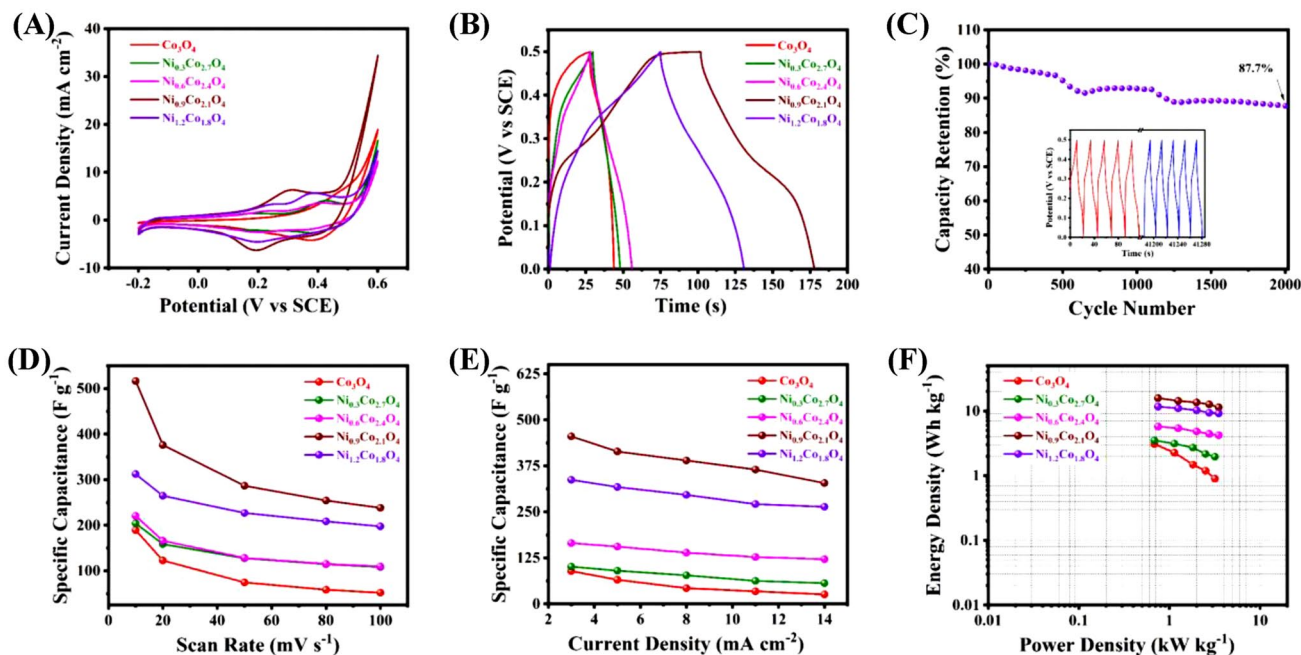


Fig. 4 Supercapacitor study of nickel cobalt oxide powders with different Ni concentrations. **A** CVs of all nickel cobalt oxide electrodes on CC at 10 mV s^{-1} scan rate. **B** GCD study of different prepared electrodes at 3 mA cm^{-2} current density. **C** Cyclic stability of electrodes prepared by using $\text{Ni}_{0.9}\text{Co}_{2.1}\text{O}_4$ powder. Inset: First and last

five cycles of GCD curves. **D** Estimated specific capacitance from CV vs. of scan rate. **E** Specific capacitance calculated from GCD curve vs. applied current density. **F** Ragone plot of different nickel cobalt oxide electrodes

electrochemical supercapacitor performance. The electrochemical performance is studied in 1 M KOH electrolyte. Figure 4A presents the cyclic voltammetry (CV) curves of all nickel cobalt oxide electrodes studied at a 10 mV s^{-1} scan rate. The maximum capacitance values estimated from CV curves are 189.31, 204.22, 220.63, 516.51, and 312.32 F g^{-1} for Co_3O_4 , $\text{Ni}_{0.3}\text{Co}_{2.7}\text{O}_4$, $\text{Ni}_{0.6}\text{Co}_{2.4}\text{O}_4$, $\text{Ni}_{0.9}\text{Co}_{2.1}\text{O}_4$, and $\text{Ni}_{1.2}\text{Co}_{1.8}\text{O}_4$ electrodes, respectively. All CVs, along with different scan rates, are mentioned in Fig. S1(A–E). From the graphs in Fig. S1, it is clear that with an increase in scan rate, the area under the curve increases as the current drawn increases with the voltage in the CV graph. But increase in scan rate limits the interaction time between electrolyte and electrode. This limited-time interaction between the electrode and electrolyte also limits the utilization of the active surface area of the electrode. Hence specific capacitance decreases with the increase in scan rate [43].

The galvanostatic charge–discharge curves are displayed in Fig. 4B of different nickel cobalt oxide electrodes studied at a current density of 3 mA cm^{-2} . The maximum specific capacitance values estimated from GCD curves are 89.10, 101.27, 165.38, 455.27, and 337.01 F g^{-1} for Co_3O_4 , $\text{Ni}_{0.3}\text{Co}_{2.7}\text{O}_4$, $\text{Ni}_{0.6}\text{Co}_{2.4}\text{O}_4$, $\text{Ni}_{0.9}\text{Co}_{2.1}\text{O}_4$, and $\text{Ni}_{1.2}\text{Co}_{1.8}\text{O}_4$ electrodes, respectively. All GCD study with various current densities is mentioned in Fig. S2(A–E). The cyclic stability is measured for the $\text{Ni}_{0.9}\text{Co}_{2.1}\text{O}_4$ electrode as it exhibited a higher capacitance value than other nickel cobalt oxide nanostructured electrodes. The observed stability for the $\text{Ni}_{0.9}\text{Co}_{2.1}\text{O}_4$ electrode is 87.7% over the 2000 charging–discharging cycles as depicted in Fig. 4C. The inset image of Fig. 4C shows the first and last charging and discharging cycles. The higher specific capacitance and stability of $\text{Ni}_{0.9}\text{Co}_{2.1}\text{O}_4$ electrode may be due to micro sheets covering nanospheres like morphology. The micro sheets and

nanosphere morphology provide maximum surface area so that the interaction between electrode and electrolyte becomes easier, enhancing the specific capacitance value. The calculated specific capacitance from CV vs. scan rate is mentioned in Fig. 4D. In contrast, the variation of specific capacitance vs. current density is mentioned in Fig. 4E. Figure 4F presents the Ragone plot. The maximum energy density for the $\text{Ni}_{0.9}\text{Co}_{2.1}\text{O}_4$ electrode is 15.81 Wh kg^{-1} (at 0.75 kW kg^{-1} power density).

The total capacitance of an electrode includes surface-controlled capacitive process (ion adsorption/desorption) and diffusion-controlled charge storage (fast faradaic redox reaction of redox species) [44]. Hence, to study detailed charge storage behavior of different prepared samples, we performed the kinetics based on CV measurement. The relationship between current (i) and scan rate (ν) is as follows [45],

$$i = a\nu^b, \quad (1)$$

where i is current at specific voltage, ν is the scan rate, a and b are constants. The values of b for surface-controlled capacitive process and diffusion-controlled process are 1 and 0.5, respectively. Figure 5A shows the plot of peak currents of different electrodes plotted against the scan rate at a fixed potential. The obtained values of b for Co_3O_4 , $\text{Ni}_{0.3}\text{Co}_{2.7}\text{O}_4$, $\text{Ni}_{0.6}\text{Co}_{2.4}\text{O}_4$, $\text{Ni}_{0.9}\text{Co}_{2.1}\text{O}_4$, and $\text{Ni}_{1.2}\text{Co}_{1.8}\text{O}_4$ electrodes are 0.71, 0.81, 0.8, 0.82, and 0.85, respectively. Hence, the values of b for all electrodes lie between 0.5 and 1 indicating mixed surface-controlled as well as diffusion-controlled processes. The exact capacitive and diffusion-controlled contribution at fixed scan rate is determined by following equation,

$$i = k_1(\nu) + k_2(\nu^{1/2}), \quad (2)$$

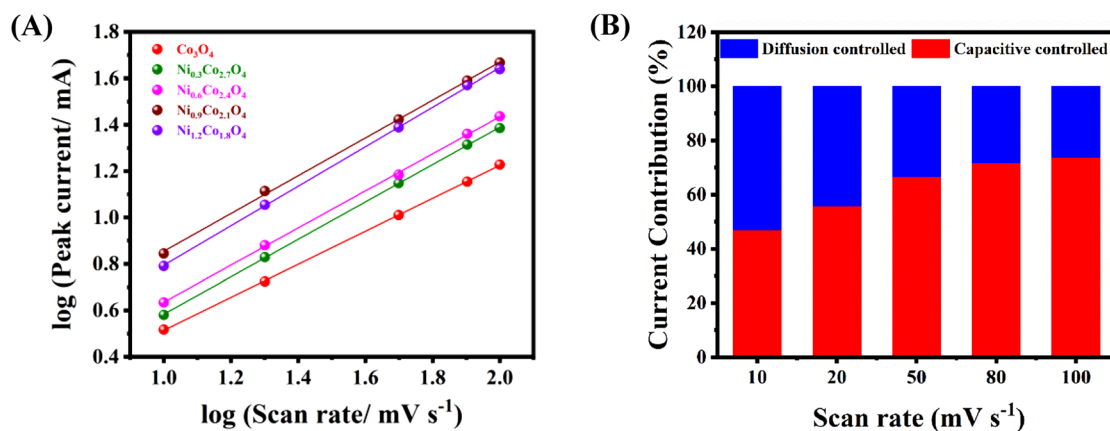


Fig. 5 Charge storage kinetics of different nickel cobalt oxide electrodes **A** Peak currents plotted against the scan rate to determine the b value. **B** The capacitive and diffusion contribution to the total charge storage of $\text{Ni}_{0.9}\text{Co}_{2.1}\text{O}_4$ electrode

where k_1 and k_2 are equation parameters and their values can be found by the slope and intercept of graph ($i\nu^{1/2}$ vs $\nu^{1/2}$), respectively (Fig. S3(A)). The capacitive and diffusion-controlled contributions in the $\text{Ni}_{0.9}\text{Co}_{2.1}\text{O}_4$ electrode are mentioned in Fig. 5B. The surface-controlled capacitive contributions for $\text{Ni}_{0.9}\text{Co}_{2.1}\text{O}_4$ electrode are 47.05%, 55.94%, 66.75%, 71.75%, and 73.91% at 10, 20, 50, 80, and 100 mV s^{-1} , respectively. Other electrodes capacitive and diffusion-controlled contributions are mentioned in Fig. S3(B–F). In case of all electrodes, it is observed that the capacitive behavior increases with scan rate. The comparison of the supercapacitor performance of present work and previously reported work is mentioned in Table 1.

3.6 Nonenzymatic glucose biosensing study

Here, the same three-electrode system is used for the glucose-sensing study except for 0.1 M NaOH electrolyte. Figure 6A–E presents the CVs of Co_3O_4 , $\text{Ni}_{0.3}\text{Co}_{2.7}\text{O}_4$, $\text{Ni}_{0.6}\text{Co}_{2.4}\text{O}_4$, $\text{Ni}_{0.9}\text{Co}_{2.1}\text{O}_4$, and $\text{Ni}_{1.2}\text{Co}_{1.8}\text{O}_4$ electrodes in the absence of glucose (red) and in the presence of 1.0 M glucose (blue). Figure 7A–E presents the CV curves of Co_3O_4 , $\text{Ni}_{0.3}\text{Co}_{2.7}\text{O}_4$, $\text{Ni}_{0.6}\text{Co}_{2.4}\text{O}_4$, $\text{Ni}_{0.9}\text{Co}_{2.1}\text{O}_4$, and $\text{Ni}_{1.2}\text{Co}_{1.8}\text{O}_4$ electrodes at different concentration of glucose (0.0, 0.2, 0.4, 0.6, 0.8, 1.0 M). Here we can observe that for all samples, peak currents are increased after the addition of glucose. The increase in the peak currents is explained as follows [46],

Table 1 Comparison of supercapacitor performance of synthesized Nickel cobalt oxide and previously reported work. (CC: Copper cloth, NF: Nickel foam, SS: stainless steel)

Sr. No	Electrode material	Current collector	Current density/scan rate	Specific capacitance (F g^{-1})	Electrolyte	References
1	NiCo_2O_4	NF	1 A g^{-1}	294	2 M KOH	[27]
2	Co_3O_4	SS	1 mA cm^{-2}	131	2 M KOH	[47]
3	U- NiCo_2O_4	NF	1 A g^{-1}	436.1	2 M KOH	[48]
4	Co_3O_4	NF	1 A g^{-1}	263	6 M KOH	[49]
5	Co_3O_4	SS	2.75 A g^{-1}	162	6 M KOH	[50]
6	NiCo_2O_4	NF	1 A g^{-1}	434.8	6 M KOH	[51]
7	NiCo_2O_4	NF	5 mV s^{-1}	332	2 M KOH	[52]
8	NiCo_2O_4	NF	1 A g^{-1}	372	2 M KOH	[53]
9	C/ NiCo_2O_4	NF	1 A g^{-1}	204.3	3 M KOH	[54]
10	$\text{Ni}_{0.9}\text{Co}_{2.1}\text{O}_4$	CC	10 mV s^{-1}	516.51	1 M KOH	Present work

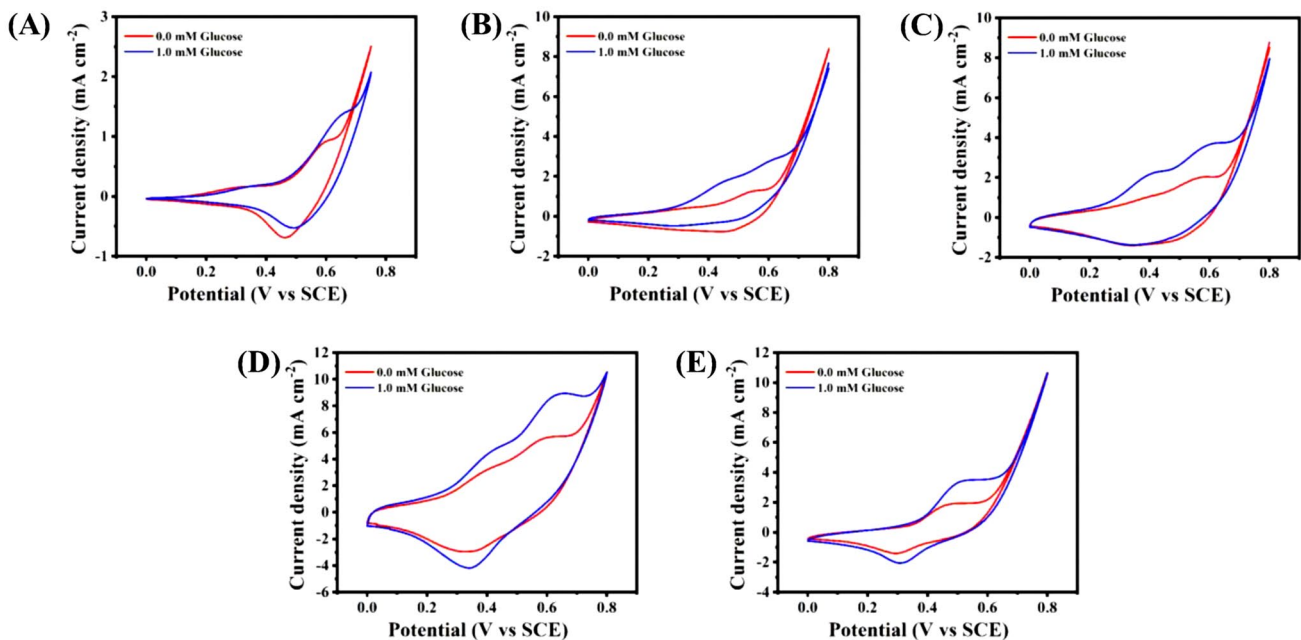


Fig. 6 Behavior of different nickel cobalt oxide electrodes on CC with and without the presence of glucose. A–E CVs of Co_3O_4 , $\text{Ni}_{0.3}\text{Co}_{2.7}\text{O}_4$, $\text{Ni}_{0.6}\text{Co}_{2.4}\text{O}_4$, $\text{Ni}_{0.9}\text{Co}_{2.1}\text{O}_4$, and $\text{Ni}_{1.2}\text{Co}_{1.8}\text{O}_4$ electrodes, respectively, with and without the presence of glucose

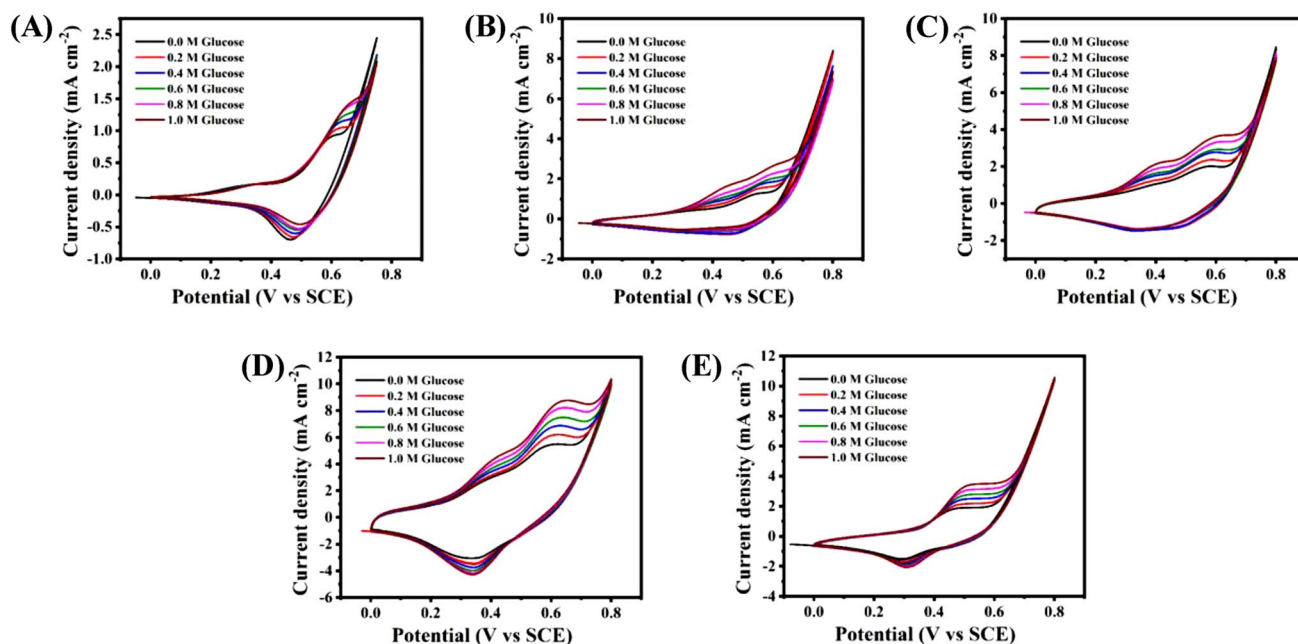
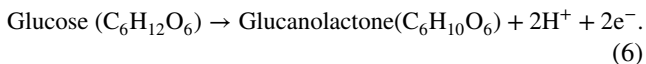
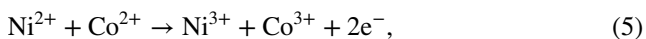
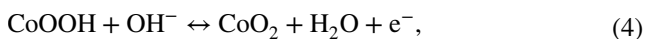


Fig. 7 A–E CV curves of Co_3O_4 , $\text{Ni}_{0.3}\text{Co}_{2.7}\text{O}_4$, $\text{Ni}_{0.6}\text{Co}_{2.4}\text{O}_4$, $\text{Ni}_{0.9}\text{Co}_{2.1}\text{O}_4$, and $\text{Ni}_{1.2}\text{Co}_{1.8}\text{O}_4$ electrodes at different concentrations of glucose at 100 mV s^{-1}



During the oxidation, Ni^{2+} and Co^{2+} ions present in the NiOOH and CoOOH compounds oxidize to Ni^{3+} and Co^{3+} with the release of two electrons (Eq. 1–3). After adding glucose, the glucose molecules dissociate and are converted into gluconolactone with the release of two electrons (Eq. 4). During reduction, the oxidized species Ni^{3+} and Co^{3+} reduce back to the Ni^{2+} and Co^{2+} by accepting electrons and returning to their original states. Figure 8A–E presents the CV of different nickel cobalt oxide electrodes in the presence of 1.0 M glucose at various scan rates (10 – 100 mV s^{-1}). It can be seen that with the scan rate, the anodic and cathodic peaks also increase. Figure 9A–E presents

the chronoamperometry study (I vs. t) of each nickel cobalt oxide electrode at 0.4 V applied potential with the subsequent addition of 0.05 mM glucose into 0.1 M NaOH electrolyte. The inset of Fig. 9A–E shows their calibration curves of Amperometric responses. The observed sensitivities for Co_3O_4 , $\text{Ni}_{0.3}\text{Co}_{2.7}\text{O}_4$, $\text{Ni}_{0.6}\text{Co}_{2.4}\text{O}_4$, $\text{Ni}_{0.9}\text{Co}_{2.1}\text{O}_4$, and $\text{Ni}_{1.2}\text{Co}_{1.8}\text{O}_4$ electrodes are 370.7 , 759.5 , 747.4 , 557.7 , $688.1 \mu\text{A mM}^{-1} \text{ cm}^{-2}$, respectively. The Nyquist plots in the absence of glucose and in the presence of 1.0 mM glucose are shown in supplementary information Fig. S4. The estimated glucose-sensing parameters are given in Table 2. As shown in Fig. 10A–E, the selectivity of samples was examined by the addition of 0.2 mM glucose and other interfering species [0.0125 mM of uric acid (UA), Ascorbic acid (AA), Fructose (FR), Sucrose (SA), and Lactic acid (LA)]. All the electrodes showed a negligible effect of interfering species as compared to glucose. The response times for all prepared electrodes are mentioned in Fig. S5 (Supplementary data). The comparative glucose-sensing study of current work and previously reported work is mentioned in Table 3.

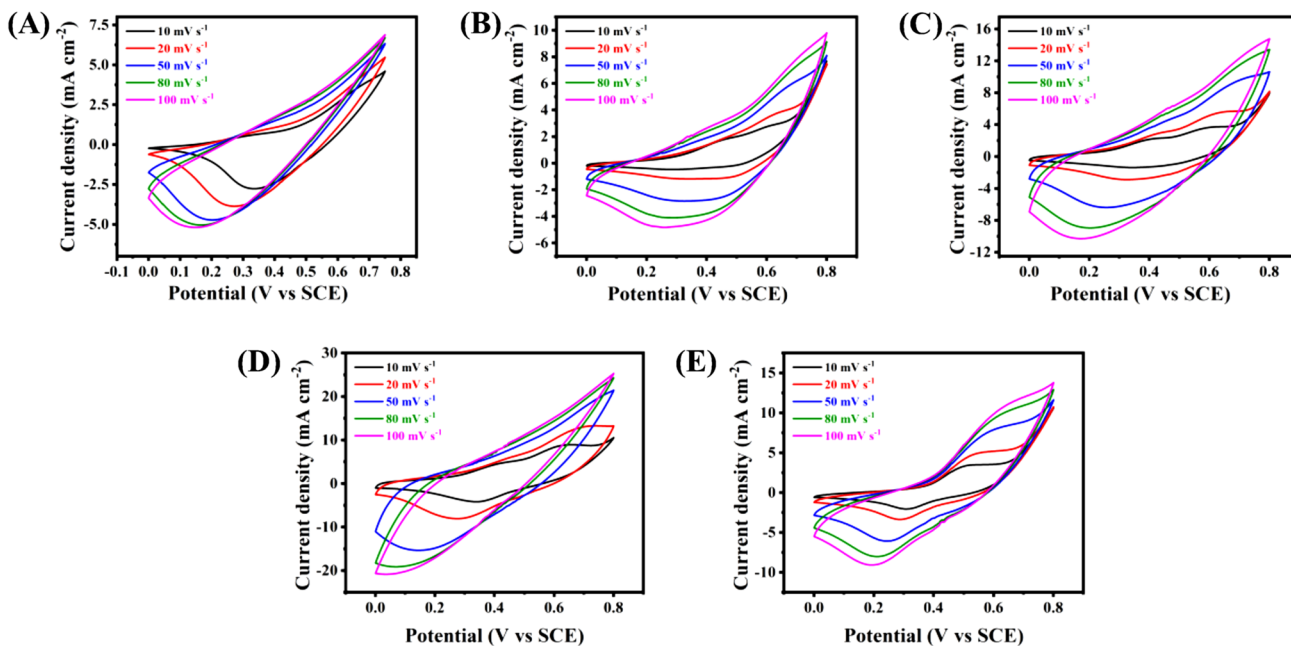


Fig. 8 A–E CVs of Co_3O_4 , $\text{Ni}_{0.3}\text{Co}_{2.7}\text{O}_4$, $\text{Ni}_{0.6}\text{Co}_{2.4}\text{O}_4$, $\text{Ni}_{0.9}\text{Co}_{2.1}\text{O}_4$, and $\text{Ni}_{1.2}\text{Co}_{1.8}\text{O}_4$ electrodes in the presence of 1.0 mM glucose at 10 to 100 mV s^{-1} scan rate

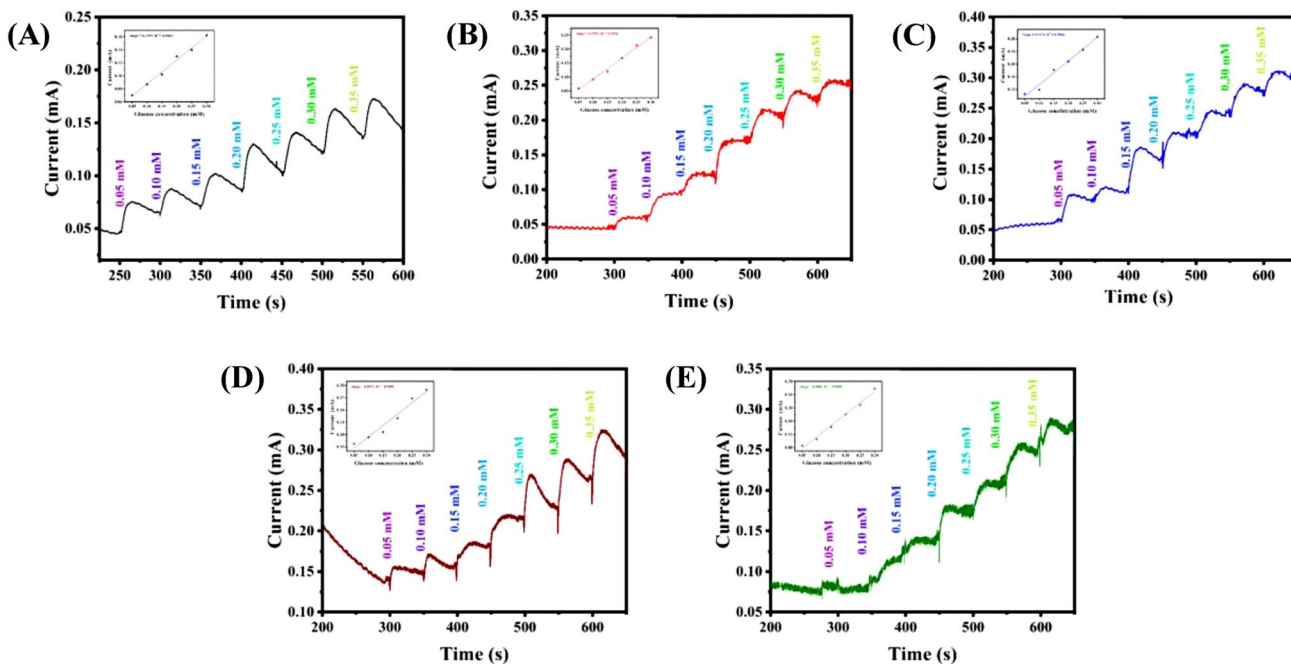


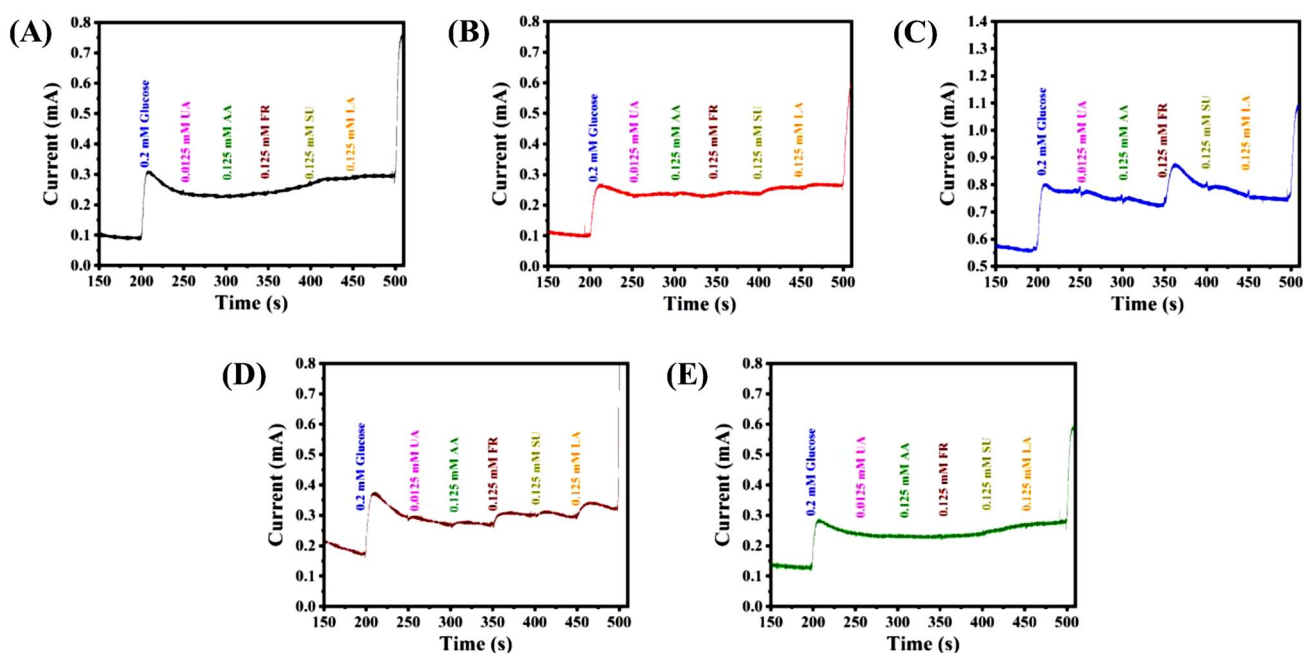
Fig. 9 A–E Amperometric responses (I vs. t) of Co_3O_4 , $\text{Ni}_{0.3}\text{Co}_{2.7}\text{O}_4$, $\text{Ni}_{0.6}\text{Co}_{2.4}\text{O}_4$, $\text{Ni}_{0.9}\text{Co}_{2.1}\text{O}_4$, and $\text{Ni}_{1.2}\text{Co}_{1.8}\text{O}_4$ electrodes at a 0.5 V potential with the addition of 0.05 mM glucose. Inset of each graph: calibration curves of chronoamperometric study]

Table 2 The estimated nonenzymatic glucose-sensing parameters of nickel cobalt oxide samples

Electrode	Sensitivity ($\mu\text{A mM}^{-1} \text{cm}^{-2}$)	Response time (s)	Correlation coefficient
Co_3O_4	370.7	15	0.9903
$\text{Ni}_{0.3}\text{Co}_{2.7}\text{O}_4$	759.5	10	0.9926
$\text{Ni}_{0.6}\text{Co}_{2.4}\text{O}_4$	747.4	18	0.9826
$\text{Ni}_{0.9}\text{Co}_{2.1}\text{O}_4$	557.7	16	0.9585
$\text{Ni}_{1.2}\text{Co}_{1.8}\text{O}_4$	688.1	11	0.9885

4 Conclusion

In summary, the nickel cobalt oxide by varying Ni concentrations has been prepared by the hydrothermal method. The nanosheet-like $\text{Ni}_{0.9}\text{Co}_{2.1}\text{O}_4$ electrode exhibited 516.51 F g^{-1} specific capacitance at 10 mV s^{-1} and cyclic stability of 87.7% over 2000 galvanostatic charge–discharge cycles. Also, it showed an energy density of 15.81 Wh kg^{-1} at 0.75 kW kg^{-1} power density. The $\text{Ni}_{0.3}\text{Co}_{2.7}\text{O}_4$ nanosheets on CC showed linear response from 0 to 0.3 mM glucose concentration and exhibited the highest glucose sensitivity of $759.5 \mu\text{A mM}^{-1} \text{cm}^{-2}$. The overall study is a platform for the development of a flexible, high-stability supercapacitor and reliable nonenzymatic glucose sensor.

**Fig. 10** A–E chronoamperometry study of (I vs. t) of Co_3O_4 , $\text{Ni}_{0.3}\text{Co}_{2.7}\text{O}_4$, $\text{Ni}_{0.6}\text{Co}_{2.4}\text{O}_4$, $\text{Ni}_{0.9}\text{Co}_{2.1}\text{O}_4$, and $\text{Ni}_{1.2}\text{Co}_{1.8}\text{O}_4$ electrodes after successive addition of glucose and interference species [UA, AA, FR, SA, and LA]**Table 3** Comparison of glucose-sensing performance of synthesized nickel cobalt oxide with previously reported work. (GCE: Glassy carbon electrode, NPs: Nanoparticles)

Sr. No	Glucose sensor	Working potential (V)	Sensitivity ($\mu\text{A mM}^{-1} \text{cm}^{-2}$)	References
1.	Co_3O_4 nanofibers-Nafion/GCE	+0.59	36.25	[55]
2.	NiCo_2O_4	+0.5	662.31	[56]
3.	NiCo_2O_4 /rGO	+0.42	548.9	[36]
4.	NiCo_2O_4	+0.5	142.14	[57]
5.	NiCo_2O_4	+0.4	27.5	[58]
6.	$\text{Ni}_{0.3}\text{Co}_{2.7}\text{O}_4$	+0.45	759.5	Present work

Supplementary Information The online version contains supplementary material available at <https://doi.org/10.1007/s00339-022-06312-3>.

Acknowledgements Authors are thankful to DST-SERB government of India for providing financial support under Early career research award Scheme File no. ECR/2017/002099.

Data availability The data will be available from the corresponding author on reasonable request.

Conflict of interest The authors declare that they have no conflict of interest.

References

- J.Y. Hwang, S.T. Myung, Y.K. Sun, *Chem. Soc. Rev.* **46**, 3529 (2017)
- V.C. Lokhande, A.C. Lokhande, C.D. Lokhande, J.H. Kim, T. Ji, *J. Alloys Compd.* **682**, 381 (2016)
- J. Yan, Q. Wang, T. Wei, Z. Fan, *Adv. Energy Mater.* **4**, 1300816 (2014)
- H. Adhikari, D. Neupane, C.K. Ranaweera, J. Candler, R.K. Gupta, S. Sapkota, X. Shen, S.R. Mishra, *Electrochim. Acta* **225**, 514 (2017)
- X. Pan, F. Ji, Q. Xia, X. Chen, H. Pan, S.N. Khisro, S. Luo, M. Chen, Y. Zhang, *Electrochim. Acta* **282**, 905 (2018)
- W.H. Low, P.S. Khiew, S.S. Lim, C.W. Siong, E.R. Ezeigwe, *J. Alloys Compd.* **775**, 1324 (2019)
- G.M. Lohar, H.D. Dhaygude, B.P. Relekar, M.C. Rath, V.J. Fulari, *Ionics* **22**, 1451 (2016)
- B.P. Relekar, A.V. Fulari, G.M. Lohar, V.J. Fulari, *J. Electron. Mater.* **48**, 2449 (2019)
- B.P. Relekar, A.V. Fulari, M.C. Rath, V.J. Fulari, G.M. Lohar, *J. Mater. Sci. Mater. Electron.* **31**, 11741 (2020)
- G.M. Lohar, O.C. Pore, A.V. Fulari, *Ceram. Int.* **47**, 16674 (2021)
- C. Liu, W. Jiang, F. Hu, X. Wu, D. Xue, *Inorg. Chem. Front.* **5**, 835 (2018)
- J. Wang, W. Dou, X. Zhang, W. Han, X. Mu, Y. Zhang, X. Zhao, Y. Chen, Z. Yang, Q. Su, E. Xie, W. Lan, X. Wang, *Electrochim. Acta* **224**, 260 (2017)
- Y. Yan, B. Li, W. Guo, H. Pang, H. Xue, *J. Power Sour.* **329**, 148 (2016)
- A.V. Fulari, M.V. Ramana Reddy, S.T. Jadhav, G.S. Ghodake, D.Y. Kim, G.M. Lohar, *J. Mater. Sci. Mater. Electron.* **29**, 10814 (2018)
- H. Zhang, M. Yao, J. Wei, Y. Zhang, S. Zhang, Y. Gao, J. Li, P. Lu, B. Yang, Y. Ma, *Adv. Energy Mater.* **7**, 1701063 (2017)
- X. Guo, K. Yan, F. Fan, Y. Zhang, Y. Duan, J. Liu, *Mater. Lett.* **240**, 62 (2019)
- C. Zhao, F. Ren, X. Xue, W. Zheng, X. Wang, L. Chang, *J. Electroanal. Chem.* **782**, 98 (2016)
- S.B. Abitkar, P.R. Jadhav, N.L. Tarwal, A.V. Moholkar, C.E. Patil, *Adv. Powder Technol.* **30**, 2285 (2019)
- D.B. Mane, O.C. Pore, R.K. Kamble, D.V. Rupnavar, S.H. Mujawar, L.D. Kadam, R.V. Dhekale, G.M. Lohar, *Appl. Phys. A* **128**, 1 (2022)
- R. Thangappan, M. Arivanandhan, R. Dhinesh Kumar, R. Jayavel, *J. Phys. Chem. Solids* **121**, 339 (2018)
- F. Wang, Y. Lai, Y. Zhang, P. Ou, P. Wu, H. Zhu, Z. Chen, S. Li, *Mater. Res. Bull.* **115**, 257 (2019)
- C. Hao, S. Zhou, J. Wang, X. Wang, H. Gao, C. Ge, *Ind. Eng. Chem. Res.* **57**, 2517 (2018)
- H. Du, Y. Li, F. Ding, J. Zhao, X.-X. Zhang, Y. Li, R. Zhao, M. Cao, T. Yu, X. Xu, *Int. J. Hydrogen Energy* **43**, 15348 (2018)
- R.B. Waghmode, H.S. Jadhav, K.G. Kanade, A.P. Torane, *Mater. Sci. Energy Technol.* **2**, 556 (2019)
- Y. Ma, Z. Yu, M. Liu, C. Song, X. Huang, M. Moliere, G. Song, H. Liao, *Ceram. Int.* **45**, 10722 (2019)
- X. Qi, W. Zheng, G. He, T. Tian, N. Du, L. Wang, *Chem. Eng. J.* **309**, 426 (2017)
- B. Saravanakumar, T. Priyadarshini, G. Ravi, V. Ganesh, A. Sakunthala, R. Yuvakkumar, *J. Sol-Gel Sci. Technol.* **84**, 297 (2017)
- S.J. Uke, G.N. Chaudhari, A.B. Bodade, S.P. Mardikar, *Mater. Sci. Energy Technol.* **3**, 289 (2020)
- S. Wu, H. Guo, L. Wang, Y. Xin, Y. Cheng, W. Fan, *Sens. Actuators B Chem.* **245**, 11 (2017)
- W. Zheng, L. Hu, L.Y.S. Lee, K.Y. Wong, *J. Electroanal. Chem.* **781**, 155 (2016)
- S. Radhakrishnan, S.J. Kim, *RSC Adv.* **5**, 44346 (2015)
- P.V. Suneesh, K. Chandhini, T. Ramachandran, B.G. Nair, T.G. Satheesh Babu, *Biosens. Bioelectron.* **50**, 472 (2013)
- Z. Qin, Q. Cheng, Y. Lu, J. Li, *Appl. Phys. A Mater. Sci. Process.* **123**, 492 (2017)
- M. Hussain, Z.H. Ibupoto, M.A. Abbasi, X. Liu, O. Nur, M. Willander, *Sensors* **14**, 5415 (2014)
- J. Yang, M. Cho, Y. Lee, *Biosens. Bioelectron.* **75**, 15 (2016)
- G. Ma, M. Yang, C. Li, H. Tan, L. Deng, S. Xie, F. Xu, L. Wang, Y. Song, *Electrochim. Acta* **220**, 545 (2016)
- J. Geng, J. Ma, S. Ma, F. Li, L. Zhang, X. Ning, G.M. Lohar, *Ceram. Int.* **45**, 14457 (2019)
- S.A. Makhlof, Z.H. Bakr, K.I. Aly, M.S. Moustafa, *Superlat. Microstruct.* **64**, 107 (2013)
- D.D.M. Prabakaran, K. Sadaiyandi, M. Mahendran, S. Sagadevan, *Appl. Phys. A Mater. Sci. Process.* **123**, 1 (2017)
- F. Liu, H. Su, L. Jin, H. Zhang, X. Chu, W. Yang, *J. Colloid Interface Sci.* **505**, 796 (2017)
- S. Liu, C. An, X. Chang, H. Guo, L. Zang, Y. Wang, H. Yuan, L. Jiao, *J. Mater. Sci.* **53**, 2658 (2018)
- P. Liu, M. Yang, S. Zhou, Y. Huang, Y. Zhu, *Electrochim. Acta* **294**, 383 (2019)
- O.C. Pore, A.V. Fulari, N.B. Velhal, V.G. Parale, H.H. Park, R.V. Shejwal, V.J. Fulari, G.M. Lohar, *Mater. Sci. Semicond. Process.* **134**, 105980 (2021)
- Y. Lan, H. Zhao, Y. Zong, X. Li, Y. Sun, J. Feng, Y. Wang, X. Zheng, Y. Du, *Nanoscale* **10**, 11775 (2018)
- A.M. Teli, S.A. Beknalkar, S.A. Pawar, D.P. Dubal, T.D. Dongale, D.S. Patil, P.S. Patil, J.C. Shin, *Energies* **13**, 6124 (2020)
- K.K. Naik, S. Kumar, C.S. Rout, *RSC Adv.* **5**, 74585 (2015)
- N. Maile, S.K. Shinde, S.S. Patil, D.Y. Kim, A.V. Fulari, D.S. Lee, V.J. Fulari, *Ceram. Int.* **46**, 14640 (2020)
- J. Wang, Y. Zhang, J. Ye, H. Wei, J. Hao, J. Mu, S. Zhao, S. Husain, *RSC Adv.* **6**, 70077 (2016)
- X. Xia, J. Tu, Y. Mai, X. Wang, C. Gu, X. Zhao, *J. Mater. Chem.* **21**, 9319 (2011)
- R. Tummala, R.K. Guduru, P.S. Mohanty, *J. Power Sources* **209**, 44 (2012)
- X. Tian, J. Dai, L. Wang, A. Xie, J. He, Y. Yan, *Mater. Technol.* **35**, 463 (2020)
- T. Kim, A. Ramadoss, B. Saravanakumar, G.K. Veerasubramani, S.J. Kim, *Appl. Surf. Sci.* **370**, 452 (2016)
- M. Kuang, W. Zhang, X.L. Guo, L. Yu, Y.X. Zhang, *Ceram. Int.* **40**, 10005 (2014)
- N.V. Nguyen, T.V. Tran, S.T. Luong, T.M. Pham, K.V. Nguyen, T.D. Vu, H.S. Nguyen, N.V. To, *ChemistrySelect* **5**, 7060 (2020)
- Y. Ding, Y. Wang, L. Su, M. Bellagamba, H. Zhang, Y. Lei, *Biosens. Bioelectron.* **26**, 542 (2010)

56. S. Cui, J. Zhang, Y. Ding, S. Gu, P. Hu, Z. Hu, *Sci. China Mater.* **60**, 766 (2017)
57. K. Jang, K.R. Park, K.M. Kim, S. Hyun, J. Jeon, Y.S. Song, S. Park, K. Moon, C. Ahn, S. Lim, J. Lee, J.C. Kim, H. Han, S. Mhin, *Nanomaterials* **11**, 55 (2020)
58. K.K. Naik, A. Gangan, B. Chakraborty, S.K. Nayak, C.S. Rout, *A.C.S. Appl. Mater. Interfaces* **9**, 23894 (2017)

Springer Nature or its licensor (e.g. a society or other partner) holds exclusive rights to this article under a publishing agreement with the author(s) or other rightsholder(s); author self-archiving of the accepted manuscript version of this article is solely governed by the terms of such publishing agreement and applicable law.

Publisher's Note Springer Nature remains neutral with regard to jurisdictional claims in published maps and institutional affiliations.